JARS Journal of Applied Remote Sensing

RESEARCH PAPER

Evaluating the potential of the Time-SIFT approach using Pléiades satellite imagery for 3D change detection

Imen Brini,[a,b,*] **Denis Feurer**,[a] **Riadh Tebourbi**,[b] **Fabrice Vinatier**,[a]
and Riadh Abdelfattah[b]
[a]UMR LISAH, Univ. Montpellier, AgroParisTech, INRAE, IRD, Institut Agro Montpellier, Montpellier, France
[b]Higher School of Communications of Tunis COSIM Lab, University of Carthage, Tunis, Tunisia

---

ABSTRACT. Optical satellite remote sensing images allow the analysis of topographic change detection based on digital elevation model differencing. Accurate change detection requires co-registration of 3D models derived from multitemporal datasets, so far, usually achieved with external reference data or manual intervention. Based on structure from motion photogrammetric algorithms, co-registering images from different epochs together by extracting multitemporal tie-points, such as the time–scale-invariant feature transform (SIFT) approach, has been proven to be efficient for aerial images. We propose a first test of the time-SIFT approach on Pléiades tri-stereoscopic satellite imagery, covering the coastal plain in northeastern Tunisia. The multitemporal tie-points, coupled with the rational polynomial coefficient models of all the images, are refined in a joint bundle adjustment routine. The accuracy of the derived digital elevation models is assessed in absolute (using external ground truth data) and relative (between epochs). The time-SIFT approach reduces the normalized median absolute deviation from 1.80 to 1.14 m when compared with the classical approach. Our results demonstrate that the time-SIFT approach can be extended for change detection analysis using Pléiades images, without ground control points or *a posteriori* co-registration, which paves the way to automated investigation of time series of past and future 3D satellite datasets. We highlight the application of the time-SIFT approach to Pléiades images leveraging their high spatial resolution for change detection.

[DOI: 10.1117/1.JRS.19.024501]

Keywords: Pléiades satellite; photogrammetry; co-registration; 3D changes

Paper 240664G received Oct. 28, 2024; revised Mar. 7, 2025; accepted Mar. 13, 2025; published Apr. 2, 2025.

---

1 Introduction

The landscape spatial patterns are continuously changing notably due to both climate change and human activities. Prior to understanding the impacts of the above-mentioned factors on landscape variation, its spatial dynamics have to be identified and assessed. Accordingly, there is a growing demand for detecting and monitoring these changes to understand their causes and their eventual consequences.

Remote change detection is one of the advanced techniques for characterizing the Earth's surface dynamics that are coupled to environmental processes at different spatial and temporal scales. The analysis of the 3D changes occurring on the Earth's surface is based on time-series

---

*Address all correspondence to Imen Brini, imen.brini@ird.fr

Handling Editor: Sicong Liu, Associate Editor

datasets acquired from different systems, including light detection and ranging (LiDAR), radar, and optical sensors.

Although LiDAR provides high-resolution point cloud data, it is hindered by its expensive cost.[1] The synthetic-aperture radar imagery has the advantage of working in all weather conditions but is affected by speckle noise and electromagnetic interference. Stereoscopic optical images are able to perceive 3D space and capture spatial details, contributing to an accurate reconstruction of the scenes.

The 3D reconstruction approaches have been categorized into two groups: traditional and learning-based approaches.[2,3] Traditional reconstruction methods are based on geometry and image processing techniques. Deep learning–based 3D reconstruction methods utilize neural networks to learn the mapping from images to 3D scenes. However, high-precision reconstruction results depend on a large amount of training data and are resource-consuming.[4]

The process of change detection aims to identify the differences between the registered 3D data. The main approaches for 3D change detection can be divided into two categories, according to the representation of the changed output: point-based and pixel-based. A direct strategy for point-based change detection is to calculate the distances between points from each point cloud, namely, cloud-to-cloud (C2C), multiscale model-to-model cloud comparison (M3C2), point-to-triangle, and point-to-plane distancing.

Often, the volume of the 3D point cloud is large, which can be difficult to process. By projecting the 3D point cloud into 2.5D data forms such as a digital elevation model (DEM), a 2D image matrix is obtained where each pixel encodes height information. Accordingly, 2D change detection methods can be applied. Change detection can be performed by DEM differencing,[5–7] requiring careful selection of the "change/no change" threshold, DEM rationing, change vector analysis,[8–10] transformation-based approaches such as principle component analysis, and classification-based approaches.[11,12]

Both, point-based and pixel-based change detection, have also been treated as a learning-based classification problem, although they require a moderate to large amount of training data and computing resources.[13]

Accordingly, optical satellite systems have made considerable advancements enabling the production of high-resolution products with minimal error. Among them, the Pléiades satellite, comprising Pléiades-1A and Pléiades-1B, was launched in 2011 and 2012, respectively. Pléiades satellite is able to acquire three-stereo images, with a push-broom sensor, allowing 3D reconstruction of the scene. The Pléiades images are supplied with rational polynomial coefficients (RPCs), which are a standard product provided by satellite data vendors that embed necessary information for DEM generation. The RPC is a projection function that relates the image to the object space.

In computer vision, the structure from motion (SfM) algorithm, based on the digital photogrammetric technique, produces stereo reconstruction that relies almost exclusively on image information and camera models to iteratively solve the camera parameters (interior and exterior orientation)[14] using thousands of automatically detected feature matches between overlapping images, based on key point detection algorithms.

The main difference between typical vision workflows and satellite stereo workflows is the camera model (pinhole versus RPCs). Frame cameras, commonly modeled using the pinhole camera model, are characterized by a central perspective projection. The relationship between the object space and image space is rigorously described by the collinearity equations, which account for the interior orientation (camera geometry) and exterior orientation (position and rotation relative to the object space). However, in the case of the Pléiades satellite, the physical-mathematical model is defined with the central perspective projection in the across-track direction and the orthogonal projection in the along-track direction. Given that the collinearity equations describing this model are complex, they are replaced by the RPCs[15] for the 3D reconstruction. According to Oh and Lee,[16] the RPCs assure an absolute geo-location accuracy of some meters.

However, for change detection, the relative accuracy of multitemporal datasets is more important than the absolute geo-location, as pointed out, for instance, by Li et al.[17] In the same context, comparing two datasets acquired in different times requires precise spatial co-registration, which is commonly executed *a posteriori*. In fact, insufficient spatial fit generates uncertainties leading to the identification of artifact changes.[18,19]

Previous studies, with frame cameras and pinhole models, have shown that joining multi-epoch datasets during the 3D reconstruction workflow will optimize the image co-registration using tie points covering several surveys and consequently impose a common geometry.[5,17] As stated by Feurer and Vinatier,[5] the abovementioned method resulted in consistent geometric reference of 3D models, and consequently, accurate DEMs of difference (DoDs), with exclusively image information.

Over time, after the "United Bundle Adjustment" proposed in 2017 by Li et al.[17] and the "time-SIFT" method proposed in 2018 by Feurer and Vinatier,[5] extensive literature has developed on this approach referring to it by different terminologies, namely "co-alignment" by Cook and Dietze,[20] "global bundle adjustment" by Garieri et al.,[21] "Multi-epoch single-imagery" by Blanch et al.,[22] "Historical SfM multiple dates—multiple blocks (4D SfM) mode" by Knuth et al.,[23] and "multitemporal SfM" by Scaioni et al.[24] These authors proved that the co-alignment of multitemporal images without using ground control points (GCPs) produces approximately the same distribution of measured changes when compared with the classical approach using GCPs. Regardless of the different terminology adapted by the authors, the above-mentioned approach, herein referred to as the time-SIFT approach, relies on extracting multitemporal tie-points and performing a common bundle adjustment. Moreover, it is worth noting that all the references using time-SIFT approaches were conducted on data acquired with frame cameras.

To the best of our knowledge, such an approach with a common bundle adjustment with push-broom sensors has not yet been studied. As stated before, the existing literature about time-SIFT approaches all used frame cameras.[5,17,20–24] Frame cameras capture the entire scene in a single exposure, simplifying the geometry and calibration processes in photogrammetric applications. Consequently, common bundle adjustment techniques have been extensively applied and studied in this context. By contrast, push-broom sensors acquire imagery line by line as the sensor moves, introducing unique challenges related to varying viewing geometries, time-dependent distortions, and sensor orientation. However, the uses of push-broom sensors for 3D change monitoring are numerous in the literature, but none of them have applied the time-SIFT approach (see details in Sec. 2 below). Hence, we propose to experiment with the time-SIFT approach using Pléiades images to produce time-series DEMs and DoDs.

The overarching goal of this study is to explore the potential of the time-SIFT approach on multitemporal stereo satellite imagery to detect 3D change with a case study using multitemporal Pléiades satellite images in the context of a Mediterranean agricultural landscape.

From this point on, the paper is structured as follows: Sec. 2 provides a brief overview of state-of-the-art of the Earth's surface change detection based on Pléiades satellite imagery; Sec. 3 represents the method; Sec. 4 describes the experimental results and discussion; and finally, the conclusion is in Sec. 5.

2 Related Work

In remote sensing and photogrammetry, RPCs describe the imaging geometry model for transforming image pixel coordinates to map coordinates. The projection function of an RPC model is formulated as follows:[25]

$$p = \frac{P_1(\phi, \lambda, h)}{P_2(\phi, \lambda, h)}, \tag{1}$$

$$r = \frac{P_3(\phi, \lambda, h)}{P_4(\phi, \lambda, h)}, \tag{2}$$

where ϕ, λ, and h represent respectively the longitude, latitude, and altitude of a 3D point, and p and r are the image coordinates. P_i is the nominator and denominator functions of the RPC equations, which are defined by

$$P(\phi, \lambda, h) = \textstyle\sum_{i=0}^{m_1} \sum_{j=0}^{m_2} \sum_{k=0}^{m_3} a_{ijk} \phi^i \lambda^j h^k , \quad \text{with } i + j + k \leq 3, \tag{3}$$

where a_{ijk} is the polynomial coefficient that approximates the sensor model information to relate the ground point coordinates to the image pixel coordinates, usually provided by the product vendor.

However, the RPCs represent some inaccuracies due to some measurement errors in attitude angle, position, and velocity that characterize the sensor. These errors can cause significant projection errors, leading to inconsistencies in different views of a scene. Such systematic errors degrade the accuracy of 3D models reconstructed from multiple views. Consequently, the RPCs require some refinement. In the literature, the two main approaches for refining the RPCs are the direct and indirect approaches. The direct approaches adjust the original RCP coefficients with some GCPs for example, whereas the indirect approaches add complementary correction functions defined in the object space or image space to correct the camera models.[26,27]

For the direct approaches, Kaichang et al.[28] proposed directly recomputing a new RPC based on a large number of GCPs that has been later on proven unfeasible by Grodecki and Dial[29] and Hu et al.[30] Other direct approaches such as the batch iterative least squares and the incremental discrete Kalman filtering require a significant number of GCPs and covariance matrices of the RPC, which are not always available to users.[31] In addition, applying the pseudo GCP method and the Using Parameters Observation Equation method proposed by Bang et al.[32] involves the challenge of properly assigning the weightings for many different observation equations.

Although direct approaches attempt to refine RPCs using GCPs, they face some limitations, such as the requirement for a large number of GCPs or the availability of covariance matrices. These constraints have led to the development of three different indirect approaches. Fraser and Hanley[33] and Grodecki and Dial[29] proposed the bias compensation method that is based on a polynomial model defined in the image space to correct the RPC. Grodecki and Dial[29] proposed a polynomial model defined in the domain of object coordinates to correct the RPC, and Kaichang et al.[28] proposed a polynomial model defined in the domain of object coordinates to correct the ground coordinates derived from the vendor-provided RPC's. In terms of accuracy, the indirect approaches are more accurate than the direct approaches.[25]

Among the indirect approaches, the bias compensation method outperforms the polynomial models defined in the domain of object coordinates as in object space, the ground coordinates do not reflect the satellite sensor's imaging geometry. Consequently, it is the most commonly used method[15,27,34] that aims to minimize the reprojection error of the tie points. For a set of N 3D points $\{X_n\}_{n=1,\dots,N}$ and their corresponding 2D observations x_{mn} across M cameras with projection functions $\{P_m\}_{m=1,\dots,M}$, the bundle adjustment finds the optimal solution by minimizing the reprojection error

$$E(P_m, X_n) = \sum_{n=1}^{N}\sum_{m=1}^{M} \|x_{mn} - P_m(X_n)\|^2, \tag{4}$$

where X_n and P_m contain the variables to be adjusted.

The reprojection error is typically defined as the sum of squared Euclidean distances between the estimated reprojected 3D points, $P_m(X_n)$, and their actual 2D observations in the images, x_{mn}.

After running the bundle adjustment, every tie point projected across different cameras is expected to be in the corresponding 2D geo-location in the images, and consequently, the corrected RPCs are consistent in a common reference frame. Once the RPCs are refined, the 3D model can be derived based on a 3D reconstruction algorithm.

Recently, the 3D reconstruction of scenes using multiple images has been widely studied for the two-view and multiview scenarios. Multiview stereo (MVS) algorithms generate a dense 3D model of the scene as a point cloud. In a typical MVS pipeline, the inputs are the robust estimations for the camera pose and the sparse points derived by SfM. To solve the correspondence search problem, many traditional and, later on, learning-based approaches have been developed. MVS algorithms may include voxel-based, surface-evolution-based, feature-point-growing-based, and depth-map-based approaches. Refer to Zhou et al.[35] for a detailed description of traditional multiview reconstruction approaches. Of the aforementioned approaches, the depth map–based approach is the most used due to its overall efficiency and scalability.[3,36]

Remote sensing–based change detection, applied in geosciences, involves different applications and allows the investigation of land surface dynamics and evolutions. Pléiades images have been widely used for deriving DEMs and estimating the changes for different environmental applications.

To assess the potential of Pléiades images in 3D reconstruction in mountainous areas, Perko et al.[37] used the RPCs to estimate the *a priori* geo-location accuracy in terms of mean and standard deviation of x and y pixel residuals compared with some ground truth datasets. For two different test sites, Trento and Innsburck, the geo-location accuracy is ∼9 and 5 m, respectively. After optimizing the sensor models with ground control points, the 3D model has a horizontal and vertical accuracy of 0.5 and 1 m, respectively.

The potential of Pléiades images for estimating vertical ground displacement after an earthquake was demonstrated by comparing derived Pléiades DEMs with pre-earthquake Lidar DEMs. Zhou et al.[38] reported a standard deviation of elevation differences of ∼0.3 m and identified meter- and sub-meter-scale offsets along fault lines, showcasing the precision of Pléiades DEMs for displacement analysis. In forested areas, a change analysis between the 2001 Ikonos stereo pair and the 2014 Pléiades stereo pair revealed height variations that were explained by the forest fire that occurred in 2007.[39]

In the context of glaciers, Pléiades images have proven effective in producing DEMs and monitoring elevation changes. After co-registering with reference altimetric data on ice-free terrain, Berthier et al.[40] evaluated the vertical precision of Pléiades-derived DEMs, highlighting their ability to achieve high accuracy, particularly for flat glacier tongues. Similarly, Deschamps-Berger et al.[41] demonstrated that Pléiades DEMs provide reliable results on stable terrain and perform well even in snow-covered areas when co-registered with NASA Airborne Snow Observatory data.

More recently, Falaschi et al.[42] utilized Pléiades DEMs from 2012 and 2020 to monitor glacier variations, achieving reliable alignment with field-surveyed checkpoints after co-registration. Berthier et al.[43] assessed Pléiades DEMs co-registered to the Copernicus GLO-30 DEM and validated them against Lidar surveys. Their study confirmed near-zero median elevation differences on and off glaciers and demonstrated the suitability of Pléiades DEMs for high-accuracy glacier change detection over various spatial scales.

In summary, according to the reviewed research, external reference data or *a posteriori* co-registration is crucial to co-register 3D models derived from multitemporal Pléiades imagery, for 3D change detection. As already mentioned, the time-SIFT approach has been proven to be efficient using aerial images, but it has not yet been implemented on satellite imagery and push-broom sensors, which is the aim of this work.

3 Method

3.1 Study Area

In the Mediterranean regions, the main sources of change in agroecosystems include vegetation dynamics, topographical factors, and anthropogenic activities. These changes occur on varying spatial and temporal scales, ranging spatially from the variability observed within the parcels to the monitoring of topographic features at the watershed level. Temporally, the study focuses on two dates, 2015 and 2018, allowing analysis of changes over a nearly 3-year interval.

The region of interest is the Lebna watershed, located in the coastal plain in northeastern Tunisia, in the Cap Bon peninsula (Fig. 1). It has an area of ∼210 km^2. The study area is characterized by a typical Mediterranean climate, and it is an agricultural region with intense plant production, including fruit culture, field crops, pastures, and olive cultivation.[44,45] Both the climate and the agricultural practices enhance the watershed vulnerability to soil erosion.[44]

Although the Lebna watershed hosts a long-term agro-hydrological observatory, providing *in situ* data,[46] remote sensing surveys cover a wide spatial extent for detecting and monitoring potential changes.

For this study, tri-stereo Pléiades imagery was ordered in 2015 and 2018 through the DINAMIS platform. The panchromatic images, with a 0.5-m resolution, are used for the DEM generation.

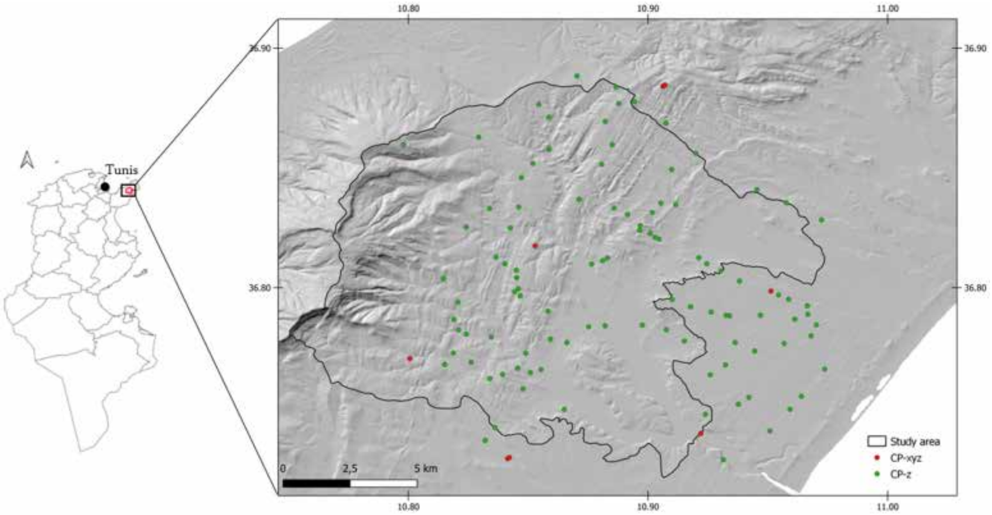

Fig. 1 Hillshaded Copernicus DEM of the study area showing the geo-location of CP_{xyz} and CP_z.

3.2 Data Processing

The time-SIFT approach has been applied to understand the effectiveness of this procedure to align satellite datasets featuring multiple characteristics and different acquisition times, compared with the classical approach. Both approaches have been examined for epoch-to-epoch image block co-registration, focusing on their performances in terms of reconstruction accuracy and processing time.

The data were processed with the free open-source software tool for photogrammetry—MicMac.[47] In the classical approach, each image block of an epoch has been independently processed to generate the DEM, following the typical SfM-MVS workflow: image alignment and dense cloud generation. The image alignment consists of tie point extraction and RPC refinement. Image tie points are extracted and matched using the SIFT algorithm[48] that is able to handle large images. In a further step, the RPCs camera models are refined in a bundle adjustment routine. MicMac resolves the RPCs refinement procedure based on the bias compensation method.[33] Two polynomial correction functions are defined in image space and estimated via a bundle block adjustment routine. Each bundle adjustment is performed with the individual images of a single epoch, i.e., individually for surveys 1 and 2. The dense cloud generation is based on the semi-global matching (SGM) algorithm. SGM provides a highly resolved topography. However, alignment errors between the point clouds are possible because they did not have exactly the same sensor orientation due to the separate bundle adjustments. Following the approach of Nuth and Kääb,[49] we compensated these alignment errors by applying the iterative closest point (ICP) algorithm on the 2018 DEM, which was co-registered onto the 2015 DEM. ICP is a frequently used algorithm for point cloud co-registration, particularly when the two clouds are already coarsely registered, which is the case here thanks to the RPC data.

On the other hand, the time-SIFT approach relies on joining all images from different epochs in the same block, hence allowing for extracting multitemporal tie points. For this step, the Agisoft Metashape Pro (v1.6.3) software package was used for multitemporal tie-point extraction, as the first experiment (not shown here) with MicMac yields almost 1% of intra-epoch tie points. The tie points extracted with Agisoft Metashape Pro were then used to continue the processing with MicMac.

The RPCs of different epochs are, as well, refined within a joint bundle adjustment routine. The result of the joint bundle adjustment is a sparse point cloud containing tie points that have been matched across overlapping frames acquired at different times. The joint bundle adjustment offers the advantage of significantly increasing the number of observations, consequently enhancing the reliability of the estimated parameters. For dense cloud generation, the images are separated into the original surveys. The computed dense models are hence—by construction—aligned in a common reference frame (during the bundle adjustment, considering

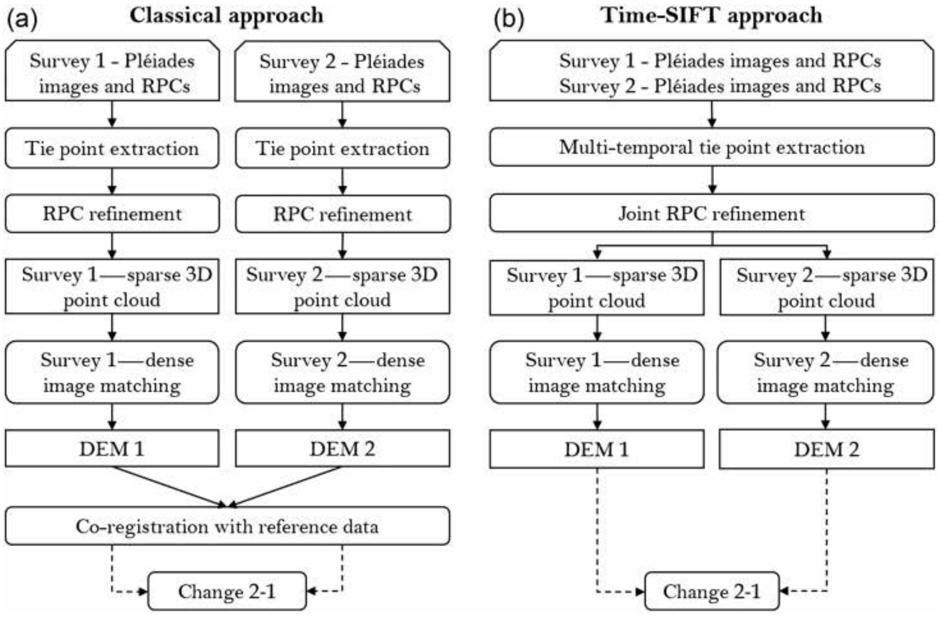

Fig. 2 Flowchart of the classical (a) and the Time-SIFT (b) approaches.

the inter-epoch tie points), and consequently, no further co-registration is required for the change detection analysis.

It is worth mentioning that no field-surveyed GCPs were used during the processing of both approaches and image information and RPCs are the unique inputs. Not employing GCPs in workflow reconstruction significantly streamlines the process, making it more efficient and thereby reducing the need for manual interventions.

Figure 2 represents the flowchart of the time-SIFT approach (b) compared with the classical approach (a).

To perform change detection, the multitemporal DEMs are subtracted to produce a pixel-level change map or DoD. The information of change is represented as a triple change mask: positive, negative, and non-change, describing the status of the change. Post-processing, such as filtering and thresholding, is required to remove false alarms, caused by noise and miss-registration.

For comparative purposes, two co-registered multitemporal Pléiades images were used to produce a residual image indicating potential changes.[50] The differences are measured from the radiometric values of the pixels. Pixels with unchanged radiance are distributed around the mean, whereas pixels with change are distributed in the tails of the distribution curve.

3.3 Data Analysis

To evaluate the time-SIFT approach performance, some metrics are used to assess its impact on the registration of 3D reconstructions from multitemporal stereo pairs.

The reprojection error [Eq. (4)] is obtained from all tie point observations in terms of Euclidean distance and expressed in pixels. It indicates the quality of the reprojection at the orientation stage.

The mean number of extracted tie-points per image pair serves as a measure of the quality of feature matching during the image alignment stage. Using the time-SIFT approach, this number compromises inter- and intra-epoch tie points.

The absolute accuracy of DEM reconstruction is determined by quantifying the residuals between some checkpoints (CP) in stable areas and their corresponding points in the derived 3D model, in terms of mean error (ME), standard deviation, and root mean square error. The absolute accuracy was quantified by manually extracting the coordinates and elevation of all CP_{xyz} (xy from the orthophoto and z from the corresponding DEM) and calculating the offset.

The relative accuracy was determined by quantifying the offset between both models in xy and z directions derived from the classical and the time-SIFT approaches. The same error statistics were estimated. The NMAD was also assessed as it is less sensitive to outliers compared with standard deviation, to compare the obtained results with results from the literature.

In stable and relatively flat areas, which mainly correspond to road surfaces, a hundred points (herein referred to as CP_z) have been manually selected through the study area and exploited for quality assessment. In the absence of systematic errors in the DEMs, areas that were unchanged during the study period are expected to be stable zones (values expected to be close to zero) in the DoD.

The absolute accuracy performed on the CP_{xyz} in terms of standard deviation is also used to estimate the minimum level of detection (LoD). This LoD is used as a threshold to distinguish real topographic change from noise. Thus, detected change below this LoD is considered noise at the chosen level of confidence.

For this purpose, the derived models were assessed for their planimetric and altimetric accuracy in absolute using 9 CP_{xyz} that were surveyed across the study area in April 2016. These data were collected using a DGPS in RTK mode, with an accuracy of 1 cm + 1 ppm for the x and y coordinates and 1.5 cm + 1 ppm for the z coordinate. All the coordinates were surveyed in the WGS 84 reference system.

For both approaches, the time required for generating the DEMs is recorded. For the classical approach, the time required to perform the co-registration process is summed up to the time required for generating the DEMs.

4 Experimental Results and Discussion

The processing of Pléiades images following the classical approach results in two DEMs of 1-m spatial resolution. The reprojection error is ∼0.54 and 0.57 pixels for DEM 2015 and DEM 2018, respectively. Both values are less than one, hence, the orientation can be considered valid data.

Before applying ICP, the DEM 2015 shows an absolute xy accuracy of ∼8.81 m on average and an absolute z accuracy of ∼2.7 m on average. For 2018 DEM, the absolute xy accuracy is ∼2.25 m on average, and the absolute z accuracy is ∼3.54 m on average (Fig. 3).

It is worth mentioning that the spatial accuracy of the Pléiades panchromatic images was estimated at 8.5 m for CE90 at the nadir direction and 10.5-m CE90 within 30-deg off-nadir when applying the provided RPC model.[51] According to Berthier et al.,[40] the Pléiades DEMs can be biased in height component by 10 to 20 m when derived without GCPs. The obtained results are consistent with the results of similar processing in the literature.[40,43]

The processing of Pléiades images following the time-SIFT approach results in two DEMs of 1-m spatial resolution. The reprojection error is ∼0.52 pixels, which is as well less than 1. The

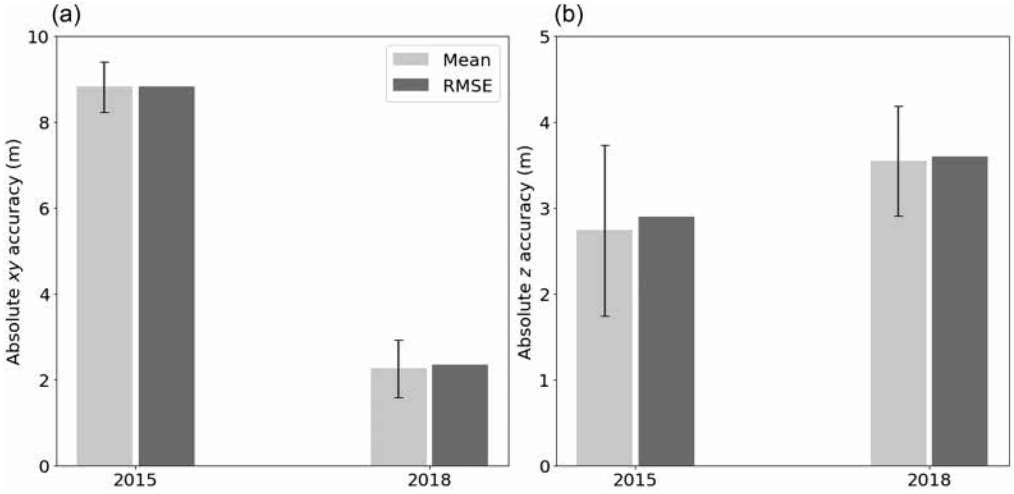

Fig. 3 Classical approach—absolute accuracy in the (a) xy direction and (b) z direction. Error bars denote the standard deviation.

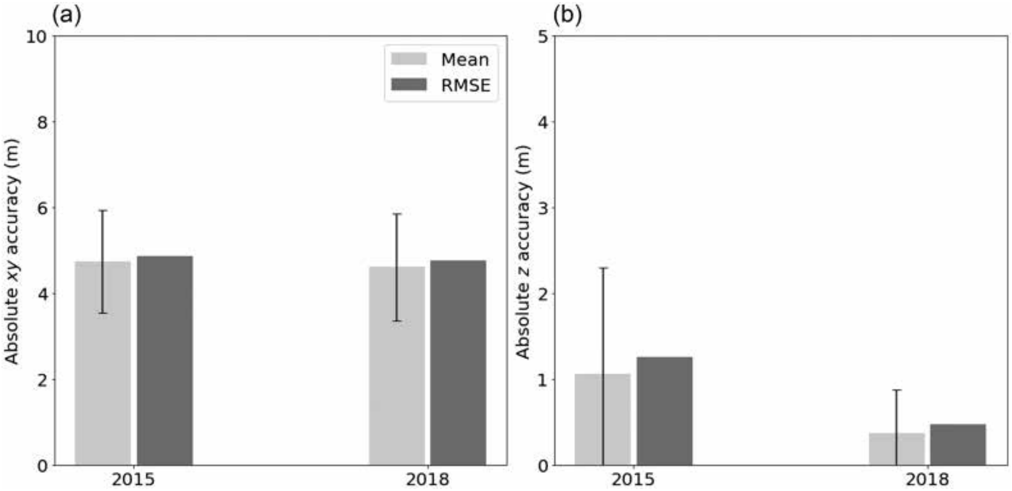

Fig. 4 Time-SIFT approach—absolute accuracy in the (a) *xy* direction and (b) *z* direction. Error bars denote standard deviation.

proportion of tie points per image pair is balanced between inter- and intra-epoch tie points. Of the total mean number of tie points per image pair, 52.50% correspond to inter-epoch tie points, and the remaining 47.49% correspond to intra-epoch tie points, ensuring accurate relative orientations.

The time-SIFT approach shows that for 2015 DEM, the absolute xy accuracy is ∼4.73 m on average and the absolute z accuracy is ∼1.05 m; and for 2018 DEM, the absolute of xy accuracy is ∼4.60 m and the absolute z accuracy is ∼0.37 m (Fig. 4).

The DoDs derived from both approaches show a systematic error in the extreme part of the study area. However, the histogram of the results from the time-SIFT approach tended mostly to 0, whereas the classical approach revealed higher deviations. This can be visualized in the DoDs and their relative histograms (Fig. 5).

The lowest range of elevation differences between both DEMs was fulfilled with the time-SIFT approach. The standard deviation of the elevation differences is reduced by almost 28%, from 1.77 in the classical approach to 1.27 m in the time-SIFT approach. The NMAD decreased with the time-SIFT approach compared with the classical approach from 1.80 to 1.14 m. These standard deviation and NMAD values are roughly equivalent in magnitude to other Pléiades DoDs used in geoscience applications. In the context of glaciers, Berthier et al.[40] found a standard deviation and an NMAD of about ±1 and ±0.5 m, respectively. Deschamps-Berger et al.[41] reported an NMAD of 0.4 m in stable terrain and 0.69 m in snow-covered areas.

Similarly, Falaschi et al.[42] reported that regardless of the seasonal snow conditions, the NMAD over off-glacier terrain remained consistently around ±1.3 m and ranged from ±0.6 to ±1.2 m in two regions of High Mountain Asia, respectively. Furthermore, Belart et al.[52] assessed the vertical bias obtained after Pléiades DEM co-registration, in terms of NMAD, revealing random errors of less than 0.5 m.

For the classical approach, using the 9 CP_{xyz}, the relative accuracy in xy direction is ∼0.65 m on average. In the z direction, the relative accuracy is ∼0.46 m on average. These findings are worthy of comparison with the results of processing Pléiades with the classical approach from literature. Previous studies reported that the relative DEM accuracy extends from 0.2 to 1 m, indicating the potential for accurate change detection over time.[40,53] For the time-SIFT approach, the relative accuracy in xy direction is ∼0.56 m on average. In the z direction, the relative accuracy is ∼0.51 m on average (Fig. 6).

The boxplots in Fig. 6 further illustrate the relative accuracy distributions for both approaches in the xy and z directions. In the xy direction [Fig. 6(a)], the median for the classical approach is 0.51 m, whereas the median for the time-SIFT approach is 0.39 m, indicating a slightly lower central tendency for the time-SIFT approach. The spread of the data, as represented by the interquartile range (IQR), is 0.36 m for the classical approach and 0.29 m for the

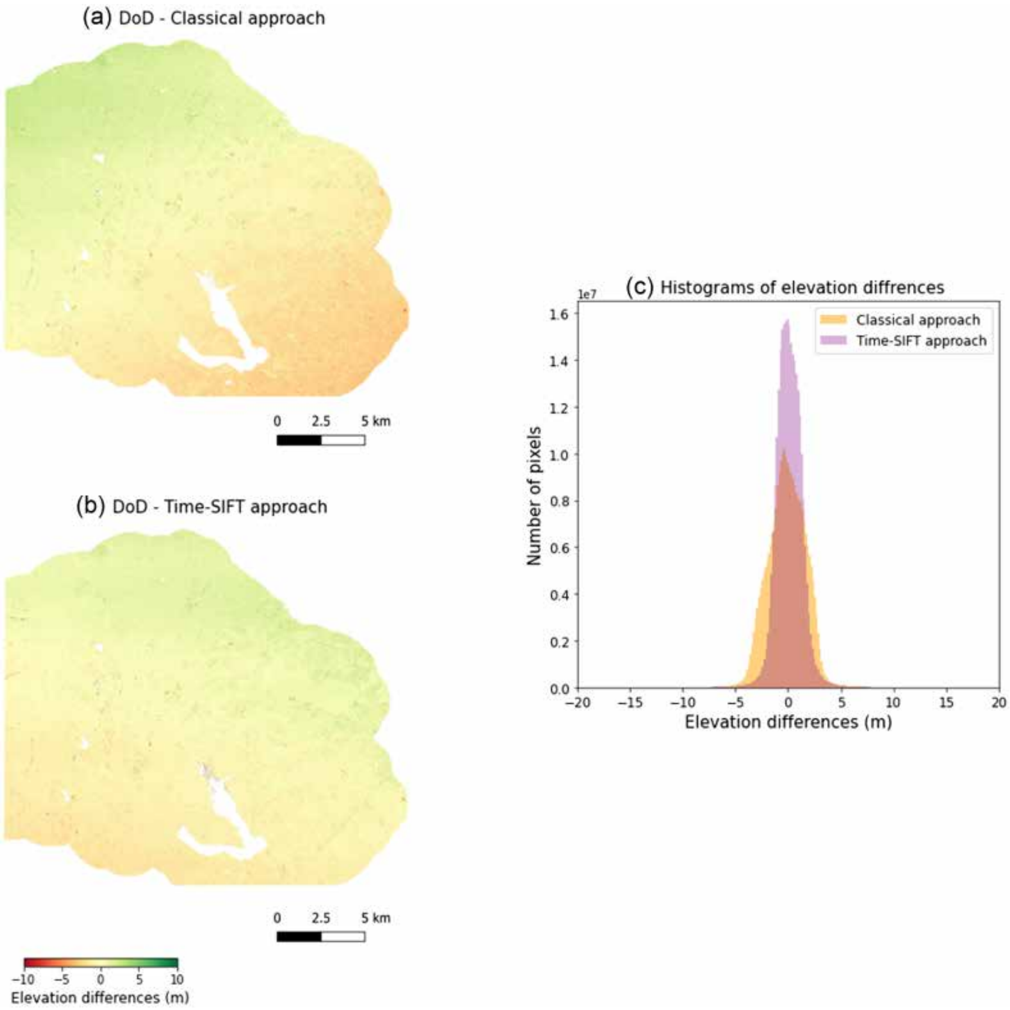

Fig. 5 Graphic representation of (a) the DoD issued from the classical approach, and (b) the DoD issued from the time-SIFT approach. (c) Histograms of the elevation differences.

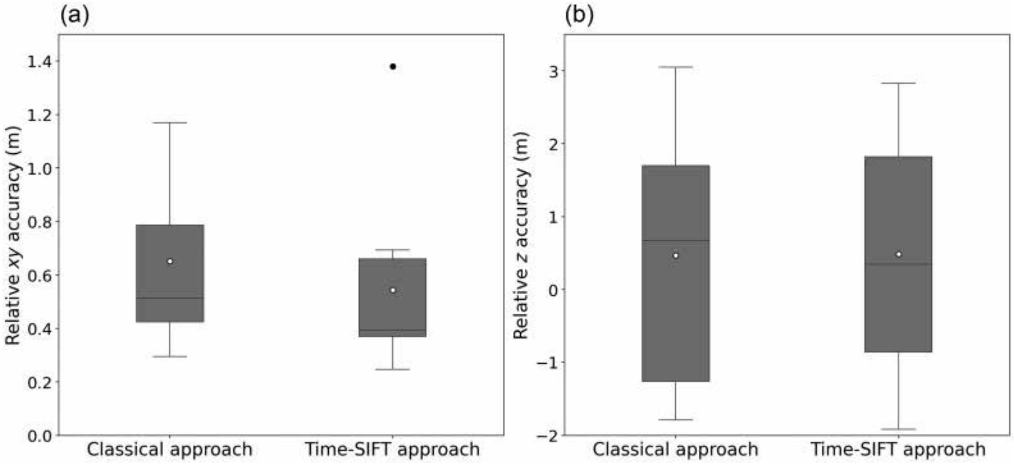

Fig. 6 Relative accuracy in (a) *xy* and (b) *z* directions for the classical and the time-SIFT approaches computed on 9 CP_{xyz} points. The horizontal lines within the boxes represent the median values, the white dots represent the mean values, and the black dots are outliers.

time-SIFT approach, suggesting less variability in the time-SIFT approach. In the z direction [Fig. 6(b)], the median for the classical approach is 0.67 m, whereas the median for the time-SIFT approach is 0.35 m, emphasizing a substantially lower central tendency for the time-SIFT approach. The IQR is 2.95 m for the classical approach and 2.67 m for the time-SIFT approach, indicating slightly reduced variability in the time-SIFT approach in the z direction.

Both approaches (classical and time-SIFT) lead to similar relative accuracy outcomes, ensuring that applying the time-SIFT approach on Pléiades imagery is relevant for change detection analysis, with no need for *a posteriori* co-registration. The difference between the relative accuracy of both approaches is not statistically significant in xy (t-test, p-value = 0.5) and z (t-test, p-value = 0.8) directions.

Further analysis of the accuracy of change detection was conducted with the CP_z. To eliminate the effect of the absolute xy offset, the residuals on CP_{xyz} are aligned with the global frame by a translation. For the classical approach, the average of the elevation differences in stable zones is −0.1 m with a standard deviation of 1.3 m. For the time-SIFT approach, the average of the elevation differences in stable zones is 0.07 m. The result aligns with the prediction that in stable zones, the elevation differences are supposed to be null or negligible. The standard deviation of the elevation differences in stable zones is ∼0.74 m (Fig. 7). The findings of the time-SIFT approach are also similar to those obtained by Ref. 54 using the classical approach with *a posteriori* co-registration. Some extreme values are also reported. These values correspond to areas that are mostly on the border of the DEMs. In these areas, noise and distortions are not well attenuated.[7]

For the classical approach, the median is −0.11 m, whereas the median for the time-SIFT approach is 0.02 m, indicating a slightly lower central tendency for the time-SIFT approach. The IQR is 1.95 m for the classical approach and 0.87 m for the time-SIFT approach, suggesting less variability in the time-SIFT approach.

The processing time has been estimated for both approaches. The classical approach takes around 10% longer duration in the processing than the time-SIFT approach. The increased time in the classical approach is mainly due to the additional step of performing the ICP. This step requires initially filtering the water bodies zones, which is not necessary in the time-SIFT approach. This filtering step adds delays to the overall process, highlighting the efficiency of the time-SIFT approach.

The exploration of the DoD derived from the time-SIFT approach exhibits different 3D change information such as man-made firewalls in a forested area, quarry excavation, and eroded zones. Figure 8 shows some detected 3D changes on the DoD, alongside the orthophotos of 2015 and 2018 and the corresponding 2D changes from Pléiades images.

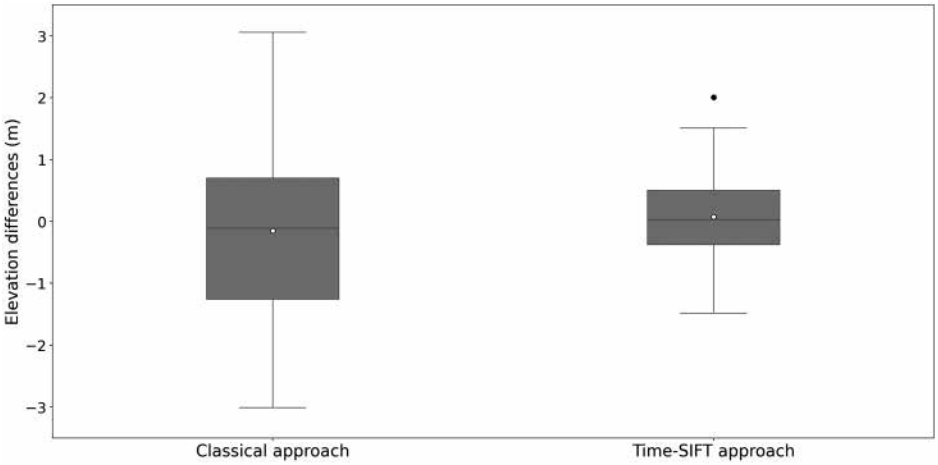

Fig. 7 Elevation differences within the CP_z situated in stable zones for the classical and the time-SIFT approaches. The horizontal lines within the boxes represent the median values, the white dots represent the mean values, and the black dots are outliers.

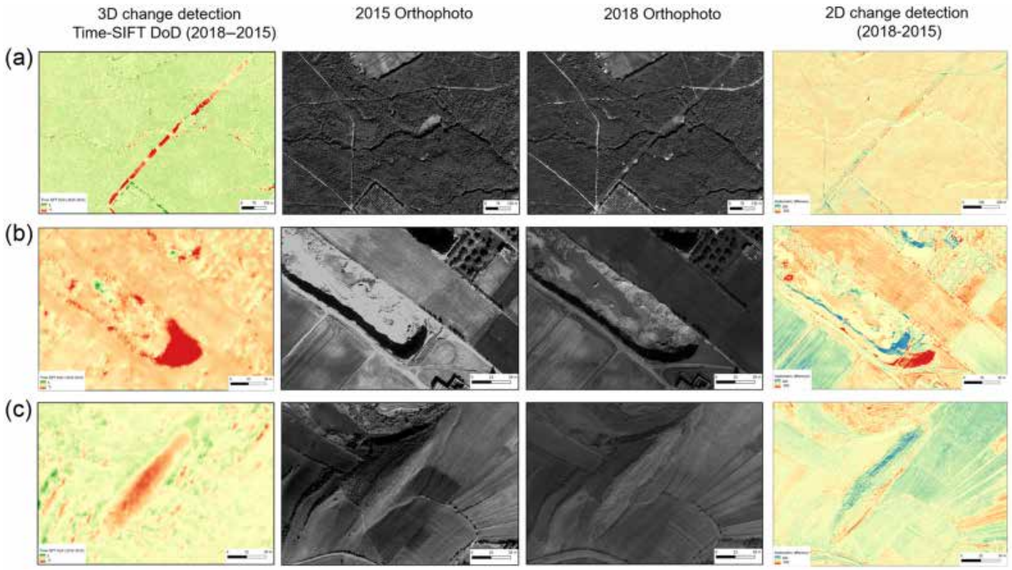

Fig. 8 Detected 3D changes on the time-SIFT DoD (left) and 2D changes on the Pléiades images (right). (a) Change associated with the man-made firewall in a forested area. (b) Change associated with quarry excavation. (c) Change associated with erosion. Contains information© CNES (2015, 2018), Distribution Airbus DS, all rights reserved. Commercial use is prohibited.

Height differencing is the most useful method for an initial check on the data quality, although it leads to potential errors. A first attempt is to examine if the subtraction could already reveal some significant changes based on the selected data; further filtering and thresholding can be developed from this point.

Although 2D change detection outlines the changes among multitemporal images, the patterns are not completely compared with those derived from the 3D change detection approach. Furthermore, 2D change detection lacks volumetric information, which is crucial for environmental monitoring.

5 Conclusion

In this work, two different co-registration approaches, applied using an open-source software tool for photogrammetry, are compared in terms of achievable accuracy and processing time. The time-SIFT approach was tested for the first time on multitemporal tri-stereo satellite imagery and showed promising results for change detection studies as it results on co-registered DEMs with no need for further *posterior* co-registration.

The accuracy of the DoD is the consequence of the generation of intra-epoch tie-points among multitemporal surveys. This finding exhibits a more accurate change detection as all the images from different surveys are refined using multitemporal tie-points and all the RPCs, resulting in a common reference system. The time-SIFT approach reveals a level of change detection comparable to that of the classical approach, with no need for *a posteriori* co-registration, and with a reduced processing time.

The main contribution of applying the time-SIFT approach to Pléiades images is its ability to reduce geometric misalignment between multitemporal satellite datasets. Accordingly, the approach can be fully automated using programming languages, hence opening the way to automated processing of past and future archives of 3D satellite acquisitions.

The success of the 3D change detection task depends on several sub-tasks, including the choice of the sensors, the selection of the 3D reconstruction approach and the registration of the 3D dataset, and finally, the 3D change detection algorithm. In this case of study, the tri-stereo Pléiades images processed with the time-SIFT approach provide valuable insights into landscape dynamics within the change detection algorithm.

Disclosures

The authors declare that there are no financial interests, commercial affiliations, or other potential conflicts of interest that could have influenced the objectivity of this research or the writing of this paper.

Code and Data Availability

The data utilized in this study were obtained from DINAMIS and cannot be shared according to the terms of the license.

Acknowledgments

This publication was made possible through support provided by the IRD.

This work has been supported by the Programme National de Télédétection Spatiale (PNTS, Grant No. PNTS-2023-05).

Data from the DINAMIS device were funded by CNES, CNRS, IGN, IRD, INRAE, and CIRAD.

For the purpose of open access, the author has applied a Creative Commons Attribution (CC BY) license to any author accepted manuscript version arising from this submission.

References

1. T. Raj et al., "A survey on LIDAR scanning mechanisms," *Electron.* **9**(5), 741 (2020).
2. M. Aharchi and M. Ait Kbir, "A review on 3D reconstruction techniques from 2D images," in *Innov. Smart Cities Appl. Ed. 3: Proc. 4th Int. Conf. Smart City Appl.*, Vol. **4**, pp. 510–522, Springer (2020).
3. Y. Niu et al., "Overview of image-based 3D reconstruction technology," *J. Eur. Opt. Soc.-Rapid Publ.* **20**(1), 18 (2024).
4. C. Wang et al., "Deep learning-based 3D reconstruction from multiple images: a survey," *Neurocomputing* **597**, 128018 (2024).
5. D. Feurer and F. Vinatier, "Joining multi-epoch archival aerial images in a single SfM block allows 3D change detection with almost exclusively image information," *ISPRS J. Photogramm. Remote Sens.* **146**, 495–506 (2018).
6. T. Bauman, O. Almog, and S. Dalyot, "Towards the automatic detection of geospatial changes based on digital elevation models produced by UAV imagery," *Int. Arch. Photogramm. Remote Sens. Spatial Inf. Sci.* **42**, 47–53 (2019).
7. M. Saponaro et al., "Influence of co-alignment procedures on the co-registration accuracy of multi-epoch SfM point clouds," *Int. Arch. Photogramm. Remote Sens. Spatial Inf. Sci.* **43**, 231–238 (2021).
8. F. Bovolo and L. Bruzzone, "A theoretical framework for unsupervised change detection based on change vector analysis in the polar domain," *IEEE Trans. Geosci. Remote Sens.* **45**(1), 218–236 (2006).
9. S. Saha, F. Bovolo, and L. Bruzzone, "Unsupervised deep change vector analysis for multiple-change detection in VHR images," *IEEE Trans. Geosci. Remote Sens.* **57**(6), 3677–3693 (2019).
10. C. He et al., "Detecting land-use/land-cover change in rural–urban fringe areas using extended change-vector analysis," *Int. J. Appl. Earth Obs. Geoinf.* **13**(4), 572–585 (2011).
11. R. Qin et al., "Object-based 3D building change detection on multitemporal stereo images," *IEEE J. Sel. Top. Appl. Earth Obs. Remote Sens.* **8**(5), 2125–2137 (2015).
12. D. Prince et al., "Multifeature fusion for automatic building change detection in wide-area imagery," *J. Appl. Remote Sens.* **11**(2), 026040 (2017).
13. W. Xiao et al., "3D urban object change detection from aerial and terrestrial point clouds: a review," *Int. J. Appl. Earth Obs. Geoinf.* **118**, 103258 (2023).
14. W. Linder, *Digital Photogrammetry*, Vol. **1**, Springer (2009).
15. E. Rupnik, M. Pierrot-Deseilligny, and A. Delorme, "3D reconstruction from multi-view VHR-satellite images in MicMac," *ISPRS J. Photogramm. Remote Sens.* **139**, 201–211 (2018).
16. J. Oh and C. Lee, "Automated bias-compensation of rational polynomial coefficients of high-resolution satellite imagery based on topographic maps," *ISPRS J. Photogramm. Remote Sens.* **100**, 14–22 (2015).
17. W. Li et al., "A new approach to performing bundle adjustment for time series UAV images 3D building change detection," *Remote Sens.* **9**(6), 625 (2017).
18. I. Aicardi et al., "An image-based approach for the co-registration of multi-temporal UAV image datasets," *Remote Sens.* **8**(9), 779 (2016).
19. J. E. Ball, D. T. Anderson, and C. S. Chan, "Comprehensive survey of deep learning in remote sensing: theories, tools, and challenges for the community," *J. Appl. Remote Sens.* **11**(4), 042609 (2017).

20. K. L. Cook and M. Dietze, "A simple workflow for robust low-cost UAV-derived change detection without ground control points," *Earth Surf. Dyn.* **7**(4), 1009–1017 (2019).
21. P. Garieri et al., "Multi-temporal image co-registration of UAV blocks: a comparison of different approaches," *Int. Arch. Photogramm. Remote Sens. Spatial Inf. Sci.* **43**, 9–16 (2021).
22. X. Blanch et al., "Multi-epoch and multi-imagery (MEMI) photogrammetric workflow for enhanced change detection using time-lapse cameras," *Remote Sens.* **13**(8), 1460 (2021).
23. F. Knuth et al., "Historical structure from motion (HSfM): automated processing of historical aerial photographs for long-term topographic change analysis," *Remote Sens. Environ.* **285**, 113379 (2023).
24. M. Scaioni, A. Malekian, and D. Fugazza, "Techniques for comparing multi-temporal archive aerial imagery for glacier monitoring with poor ground control," *Int. Arch. Photogramm. Remote Sens. Spat. Inf. Sci.* **48**, 293–300 (2023).
25. Z. Xiong and Y. Zhang, "A generic method for RPC refinement using ground control information," *Photogramm. Eng. Remote Sens.* **75**(9), 1083–1092 (2009).
26. E. Rupnik et al., "Refined satellite image orientation in the free open-source photogrammetric tools Apero/MicMac," *ISPRS Ann. Photogramm. Remote Sens. Spat. Inf. Sci.* **III-1**, 83–90 (2016).
27. R. Marí et al., "A generic bundle adjustment methodology for indirect RPC model refinement of satellite imagery," *Image Process. Online* **11**, 344–373 (2021).
28. D. Kaichang, M. Ruijin, and L. Rong Xing, "Rational functions and potential for rigorous sensor model recovery," *Photogramm. Eng. Remote Sens.* **69**(1), 33–41 (2003).
29. J. Grodecki and G. Dial, "Block adjustment of high-resolution satellite images described by rational polynomials," *Photogramm. Eng. Remote Sens.* **69**(1), 59–68 (2003).
30. Y. Hu, V. Tao, and A. Croitoru, "Understanding the rational function model: methods and applications," *Int. Arch. Photogramm. Remote Sens.* **20**(6), 119–124 (2004).
31. Y. Hu and C. V. Tao, "Updating solutions of the rational function model using additional control information," *Photogramm. Eng. Remote Sens.* **68**(7), 715–724 (2002).
32. K. I. Bang et al., "Automatic DEM generation using IKONOS stereo imagery," in *IGARSS 2003. IEEE Int. Geosci. Remote Sens. Symp. Proc.*, Vol. **7**, IEEE, pp. 4289–4291 (2003).
33. C. S. Fraser and H. B. Hanley, "Bias compensation in rational functions for IKONOS satellite imagery," *Photogramm. Eng. Remote Sens.* **69**(1), 53–57 (2003).
34. R. Marí et al., "Automatic stockpile volume monitoring using multi-view stereo from SkySat imagery," in *IEEE Int. Geosci. Remote Sens. Symp. (IGARSS)*, IEEE, pp. 4384–4387 (2021).
35. L. Zhou et al., "DP-MVS: detail preserving multi-view surface reconstruction of large-scale scenes," *Remote Sens.* **13**(22), 4569 (2021).
36. E. K. Stathopoulou and F. Remondino, "A survey on conventional and learning-based methods for multi-view stereo," *Photogramm. Rec.* **38**(183), 374–407 (2023).
37. R. Perko et al., "Assessment of the mapping potential of Pléiades stereo and triplet data," *ISPRS Ann. Photogramm. Remote Sens. Spat. Inf. Sci.* **2**, 103–109 (2014).
38. Y. Zhou et al., "Assessing the ability of Pléiades stereo imagery to determine height changes in earthquakes: a case study for the El Mayor–Cucapah epicentral area," *J. Geophys. Res.: Solid Earth* **120**(12), 8793–8808 (2015).
39. D. Akca et al., "Volumetric forest change detection through VHR satellite imagery," in *Int. Arch. Photogramm. Remote Sens. Spat. Inf. Sci.: XXIII ISPRS Congress*, pp. 1213–1220 (2016).
40. E. Berthier et al., "Glacier topography and elevation changes derived from Pléiades sub-meter stereo images," *Cryosphere* **8**(6), 2275–2291 (2014).
41. C. Deschamps-Berger et al., "Snow depth mapping from stereo satellite imagery in mountainous terrain: evaluation using airborne laser-scanning data," *Cryosphere* **14**(9), 2925–2940 (2020).
42. D. Falaschi et al., "Increased mass loss of glaciers in Volcán Domuyo (Argentinian Andes) between 1962 and 2020, revealed by aerial photos and satellite stereo imagery," *J. Glaciol.* **69**(273), 40–56 (2023).
43. E. Berthier et al., "The Pléiades glacier observatory: high resolution digital elevation models and ortho-imagery to monitor glacier change," *EGUsphere* **2024**, 5551–5571 (2024).
44. I. Mekki et al., "Impact of farmland fragmentation on rainfed crop allocation in Mediterranean landscapes: a case study of the Lebna watershed in cap bon, Tunisia," *Land Use Policy* **75**, 772–783 (2018).
45. A. Gasmi et al., "Satellite multi-sensor data fusion for soil clay mapping based on the spectral index and spectral bands approaches," *Remote Sens.* **14**(5), 1103 (2022).
46. J. Molenat et al., "Omere: a long-term observatory of soil and water resources, in interaction with agricultural and land management in Mediterranean hilly catchments," *Vadose Zone J.* **17**(1), 1–18 (2018).
47. M. Pierrot Deseilligny and I. Cléry, "Apero, an open source bundle adjustment software for automatic calibration and orientation of set of images," *Int. Arch. Photogramm. Remote Sens. Spat. Inf. Sci.* **38**, 269–276 (2012).
48. D. G. Lowe, "Distinctive image features from scale-invariant keypoints," *Int. J. Comput. Vis.* **60**, 91–110 (2004).

49. C. Nuth and A. Kääb, "Co-registration and bias corrections of satellite elevation data sets for quantifying glacier thickness change," *Cryosphere* **5**(1), 271–290 (2011).
50. A. Yehia, H. Elhifnawy, and M. Safy, "Effect of different spatial resolutions of multi-temporal satellite images change detection application," in *Int. Conf. Innovative Trends Comput. Eng. (ITCE)*, IEEE, pp. 41–46 (2019).
51. E. Astrium, *Pléiades Imagery User Guide V 2.0* (2012).
52. J. Belart et al., "Winter mass balance of Drangajökull ice cap (NW Iceland) derived from satellite sub-meter stereo images," *Cryosphere* **11**(3), 1501–1517 (2017).
53. P. Lacroix, E. Berthier, and E. T. Maquerhua, "Earthquake-driven acceleration of slow-moving landslides in the Colca Valley, Peru, detected from Pléiades images," *Remote Sens. Environ.* **165**, 148–158 (2015).
54. L. Beraud et al., "Glacier-wide seasonal and annual geodetic mass balances from Pléiades stereo images: application to the Glacier d'Argentière, French Alps," *J. Glaciol.* **69**(275), 525–537 (2023).

Imen Brini is currently working toward a PhD in information and communication technologies applied to Earth and Water Sciences at the University of Carthage, Tunisia, and the University of Montpellier, France. She received her master of science degree in geoinformation in environmental management in 2021 from the Mediterranean Agronomic Institute of Chania, Chania, Greece (CIHEAM). Her research interests include remote sensing, geographic information systems, image processing, and environmental management.

Denis Feurer is currently a research scientist in Montpellier in the LISAH lab for the French Research Institute for Development (IRD). He received his engineering degree from ISAE-SUPAERO, Toulouse, France in 2002 and his PhD in geomatics and environmental science from both AgroParisTech, Paris, France in 2008 and Université Laval, Québec, Canada in 2009. His work focuses on developing remote sensing methods applied to hydrology, erosion, and monitoring of agrosystems.

Riadh Tebourbi: Biography is not available.

Fabrice Vinatier is a scientist from INRAE. He received his engineering degree in agronomy and his PhD in spatial ecology from AgroParisTech, Paris, France. He currently leads the LISAH agrosystem ecohydrology team and is involved in understanding the functioning of plant cover in Mediterranean environments. More specifically, he is developing tools and methods for mapping the diversity of plant communities in agricultural landscapes.

Riadh Abdelfattah is a researcher at the COSIM Lab at SUP'COM, and Tunisia's representative for the Climate-Neutral and Smart Cities European mission within the Horizon Europe research and innovation program (2021–2027). He obtained his engineering degree from the School of Telecommunications of Tunis in June 1995, followed by a PhD in electrical engineering from the National School of Engineers of Tunis 2000. His research focuses on AI applications in remote sensing, particularly in environmental management.